Volume 11
Number 22
14 June 2023
Pages 4823–5034

Journal of Materials Chemistry B

Materials for biology and medicine

rsc.li/materials-b

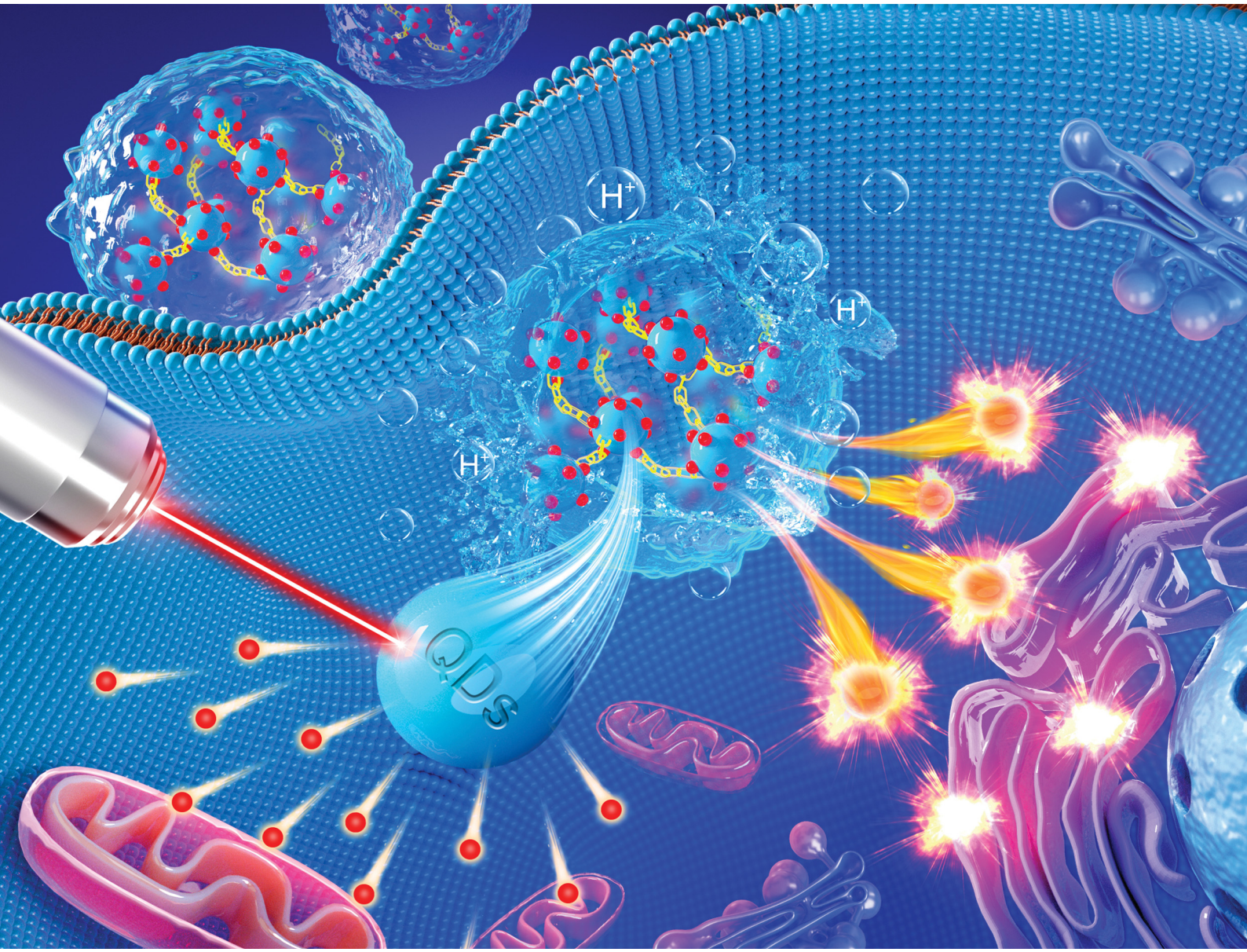

ISSN 2050-750X

ROYAL SOCIETY OF CHEMISTRY

PAPER

Aiguo Wu, Jianwei Li *et al.*

Using host–guest interactions at the interface of quantum dots to load drug molecules for biocompatible, safe, and effective chemo-photodynamic therapy against cancer

10 YEARS ANNIVERSARY

Journal of Materials Chemistry B

ROYAL SOCIETY OF CHEMISTRY

PAPER

View Article Online
View Journal | View Issue

Cite this: J. Mater. Chem. B, 2023, 11, 4855

Using host–guest interactions at the interface of quantum dots to load drug molecules for biocompatible, safe, and effective chemo-photodynamic therapy against cancer†

Xiaoxia Wu, [ae] Jinghui Yang,[ab] Jie Xing,[d] Yonglei Lyu,[ab] Ruifen Zou,[d] Xin Wang,[ab] Junlie Yao,[d] Dinghu Zhang,[e] Dawei Qi,[a] Guoliang Shao,[e] Aiguo Wu *[d] and Jianwei Li *[ac]

Combining photodynamic therapy (PDT) and chemotherapy (CHT) by loading an anti-cancer drug and a photosensitizer (PS) into the same delivery nanosystem has been proposed as an effective approach to achieve synergistic effects for a safe cancer treatment. However, exploring an ideal delivery nanosystem has been challenging, because the noncovalent interactions must be maintained between the multiple components to produce a stable yet responsive nanostructure that takes into account the encapsulation of drug molecules. We addressed this issue by engineering the interfacial interaction between Ag_2S quantum dots (QDs) using a pillararene derivative to direct the co-self-assembly of the entire system. The high surface area-to-volume ratio of the Ag_2S QDs provided ample hydrophobic space to accommodate the anti-drug molecule doxrubicine. Moreover, Ag_2S QDs served as PSs triggered by 808 nm near-infrared (NIR) light and also as carriers for high-efficiency delivery of drug molecules to the tumor site. Drug release experiments showed smart drug release under the acidic micro-environments (pH 5.5) in tumor cells. Additionally, the Ag_2S QDs demonstrated outstanding PDT ability under NIR light, as confirmed by extracellular and intracellular reactive oxygen species generation. Significant treatment efficacy of the chemo-photodynamic synergistic therapy for cancer using the co-delivery system was demonstrated *via in vitro* and *in vivo* studies. These findings suggest that our system offers intelligent control of CHT and PDT, which will provide a promising strategy for constructing hybrid systems with synergistic effects for advanced applications in biomedicine, catalysis, and optoelectronics.

Received 20th March 2023,
Accepted 25th April 2023

DOI: 10.1039/d3tb00592e

rsc.li/materials-b

Introduction

Cancer treatment remains a significant challenge to human health, and the development of new therapeutic strategies is crucial to improving patient outcomes.[1] While researchers have made progress with clinical treatments such as chemotherapy (CHT), radiotherapy, and surgery, the emergence of novel therapeutic modalities has occurred in recent years, including drug photodynamic therapy (PDT), photothermal therapy (PTT), magnetic hyperthermia, sonodynamic therapy (SDT), chemodynamic therapy (CDT), and immunotherapy.[2] However, a major issue in clinical treatment is how to increase patient survival with the use of a single treatment method, as each modality has its limitations.[3–7]

Combinatorial therapy, which involves using multiple treatment modalities, has been proposed as a method to enhance their complementarity and maximize their strengths to produce synergistic effects.[8,9] Self-assembly approaches using supramolecular

[a] MediCity Research Laboratory, University of Turku, Tykistökatu 6, FI-20520 Turku, Finland. E-mail: jianwei.li@utu.fi
[b] Department of Chemistry, University of Turku, Vatselankatu 2, FI-20014 Turku, Finland
[c] Hainan Provincial Key Laboratory of Fine Chem, School of Chemical Engineering and Technology, Hainan University, Haikou 570228, China
[d] Cixi Institute of Biomedical Engineering, International Cooperation Base of Biomedical Materials Technology and Application, Chinese Academy of Science (CAS) Key Laboratory of Magnetic Materials and Devices & Zhejiang Engineering Research Center for Biomedical Materials, Ningbo Institute of Materials Technology and Engineering, CAS, 1219 ZhongGuan West Road, Ningbo 315201, China. E-mail: aiguo@nimte.ac.cn
[e] Department of Interventional Radiology, The Cancer Hospital of the University of Chinese Academy of Sciences (Zhejiang Cancer Hospital), Institute of Basic Medicine and Cancer (IBMC), Chinese Academy of Sciences (CAS), Hangzhou 310022, China

† Electronic supplementary information (ESI) available. See DOI: https://doi.org/10.1039/d3tb00592e

concepts are promising strategies for developing delivery nanosystems[10–13] that can encapsulate quantum dots (QDs) and anticancer drugs for targeted treatment of tumor lesions. However, these approaches face significant challenges such as low stability, resulting in disassembly and payload leakage during the delivery process, uncontrollable drug release in the extracellular matrix of tumor tissue, and low efficiency in cancer treatment.[14–18] This unmet situation has been rooted in the challenge of exploring suitable supramolecular host molecules to balance the noncovalent interaction between the multiple components in the complex chemical system.[19,20]

In this study, we employed cationic pillar[6]arene (CP6) columnar molecules capable of associating with Ag_2S QDs modified with alkyl chain ligands through host–guest interactions to develop a stable and pH-responsive self-assembled co-delivery system for chemo-photodynamic cancer therapy. This system co-delivered semiconductor QDs (Ag_2S QDs) and doxorubicin (DOX) to tumors, exhibiting strong reactive oxygen species (ROS) generation capability and stimuli-responsive release of drugs and QDs in acidic microenvironments (pH 5.5).[21–23]

Ag_2S QDs were chosen for self-assembled nano-structure formation due to their ultra-small size of approximately 4 nm, which facilitated the formation of ordered structures driven by host–guest interactions.[24] The surface of Ag_2S QDs modified with a ligand possessing –COOH groups can interact with CP6, driving Ag_2S QDs to form ordered self-assembled nanostructures. This interfacial engineering can produce ample hydrophobic spaces to accommodate DOX molecules due to the high surface area-to-volume ratio of the inorganic QDs, enabling the co-delivery system to load anticancer drugs. Ag_2S QDs not only act as photosensitizers (PSs) under the excitation of 808 nm near-infrared (NIR) light, but also as nanocarriers that increase the efficiency of delivering anticancer drugs to the tumor site.[15,25] A combination of phototherapy and CHT can reduce the likelihood of tumor recurrence after PDT, and the co-delivery system with satisfactory ROS generation ability and stimuli-response of payload release can be used to achieve intelligent control of drug release for CHT, offering a synergistic effect for chemo-photodynamic therapy.

Experimental

Materials

Silver nitrate ($AgNO_3$) and ammonium sulfide ($(NH_4)_2S$) were purchased from Sigma-Aldrich. Doxorubicin (DOX) was purchased from Adamas Beta. *N*-Hydroxysuccinimide (NHS), α-lipoic acid (LA), 11-aminoundecanoic acid (11-AUA), and thiazolyl blue tetrazolium bromide (MTT) were obtained from TCI. Hoechst 33342, LysoTracker™ Deep Red and Dead Cell Apoptosis Kit with Annexin V FITC and propidium iodide (PI) for flow cytometry were purchased from Invitrogen™ and ThermoFisher Scientific. Cationic pillar[6]arene (CP6) was synthesized according to a previously reported protocol.[24]

Synthesis of Ag_2S QDs

Ag_2S QDs were synthetized by two steps. First, Ag_2S nanoparticles were prepared using a modified method.[26,27] Briefly, 1.0 mL $AgNO_3$ aqueous solution (20 mM) and 0.2 mL LA aqueous solution (20 mM) were mixed with pure water (8.3 mL) and then stirred for 10 min. Next, 0.5 mL $(NH_4)_2S$ aqueous solution (20 mM) was added to the above mixture, which was stirred for 30 min, and then stored in the dark overnight at room temperature. The obtained nanoparticles were purified by ultrafiltration using Ultra-15 centrifugal filter units (Millipore, MWCO 3.0 kDa) and redispersed in 10.0 mL of Milli-Q water. Second, for 11-AUA modification on the Ag_2S nanoparticles, NHS (0.25 mL, 20 mM) was added to the above Ag_2S nanoparticles (10.0 mL), and then stirred for 8 h. Then, 11-AUA (1.0 mL, 5 mM) was added and reacted for another 16 h. The obtained Ag_2S QDs were purified by ultrafiltration, redispersed in 5.0 mL of Milli-Q water, and stored at 4 °C in the dark.

The preparation of the co-delivery system

For the self-assembled co-delivery system (Ag_2S-DOX-CP6), 0.5 mL of Ag_2S QDs was mixed with 1 mL of phosphate-buffered saline (PBS, pH 7.4). Next, CP6 (0.2 mL, 0.1 mM) and DOX (0.3 mL, 1 mM) were added to the mixture, which was stirred for 48 h in the dark. The obtained Ag_2S-DOX-CP6 was collected by centrifugation (8000 rpm, 5 min) and redispersed in 1.0 mL H_2O (the concentration was calculated as 1.0 mg mL^{-1}).

Additionally, Ag_2S-DOX-CP6-783 nanoparticles were synthesized using a method similar to the DOX loading approach to study their performance *in vivo*. Briefly, 0.5 mL of Ag_2S QDs was mixed with 1.0 mL of PBS (pH 7.4), CP6 (0.2 mL, 0.1 mM), DOX (0.3 mL, 1 mM), and IR-783 (2 μL, 20 mM) for 48 h reaction. The obtained Ag_2S-DOX-CP6-783 was collected after centrifugation and redispersed in 1.0 mL H_2O. The stability of Ag_2S-DOX-CP6 was also estimated by dynamic light scattering (DLS) for different samples in PBS, Dulbecco's modified Eagle's medium (DMEM), and fetal bovine serum (FBS).

The details of characterization, drug release, ROS detection, biocompatibility, and chemo-photodynamic therapy methods *in vitro* and *in vivo* are provided in the ESI.†

Results and discussion

Design and synthesis of the co-delivery system

Zero-dimensional semiconductor nanomaterials, such as Ag_2S QDs, have been shown to effectively generate ROS under NIR light energy and can be combined with anti-cancer drugs for co-delivery to tumor tissues.[11–13] Thus, we selected Ag_2S QDs as a component in our combinatorial therapeutic agent designed for chemo-photodynamic treatment of cancer. We developed a self-assembled co-delivery system (Ag_2S-DOX-CP6), as illustrated in Scheme 1. First, we prepared Ag_2S QDs by reducing $AgNO_3$ with LA and $(NH_4)_2S$, followed by extending the alkyl chain of the surface ligand through the reaction between the –COOH and $–NH_2$ groups of 11-AUA, to enable effective hydrophobic interaction with DOX molecules.[28] The Ag_2S QDs

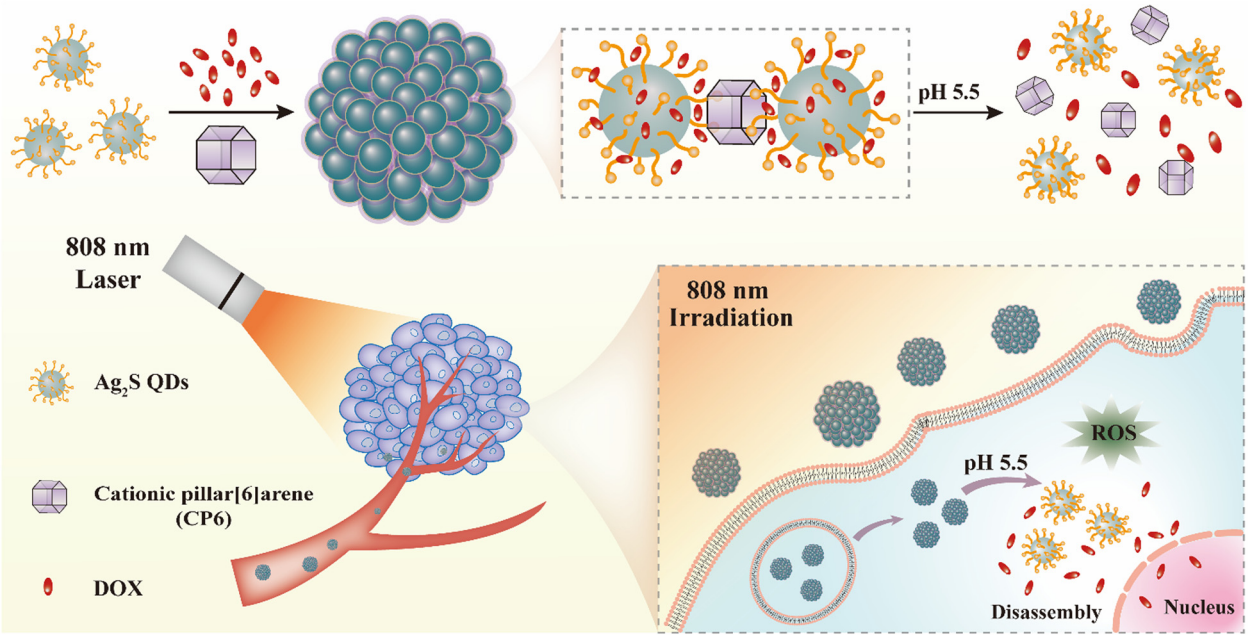

Scheme 1 A representation of the self-assembled co-delivery system (Ag_2S-DOX-CP6) based on host–guest interaction for chemo-photodynamic synergistic therapy of cancer.

modified with a carboxyl (–COOH) group were adequately dispersed in an aqueous solution due to charge repulsion between the QDs, and transmission electron microscopy (TEM) analysis showed an average diameter of approximately 4 nm (Fig. 1a). The DLS results confirmed this size with a hydrodynamic diameter of approximately 8 nm (Fig. 1b).

The negatively charged Ag_2S QDs underwent host–guest interaction with CP6, which drove the self-assembly of Ag_2S QDs into nanostructures. During the self-assembly process, DOX was loaded into the nanostructures through hydrophobic interaction between DOX and the alkyl chain on the surface of the Ag_2S QDs (Fig. 1c). The key difference between our

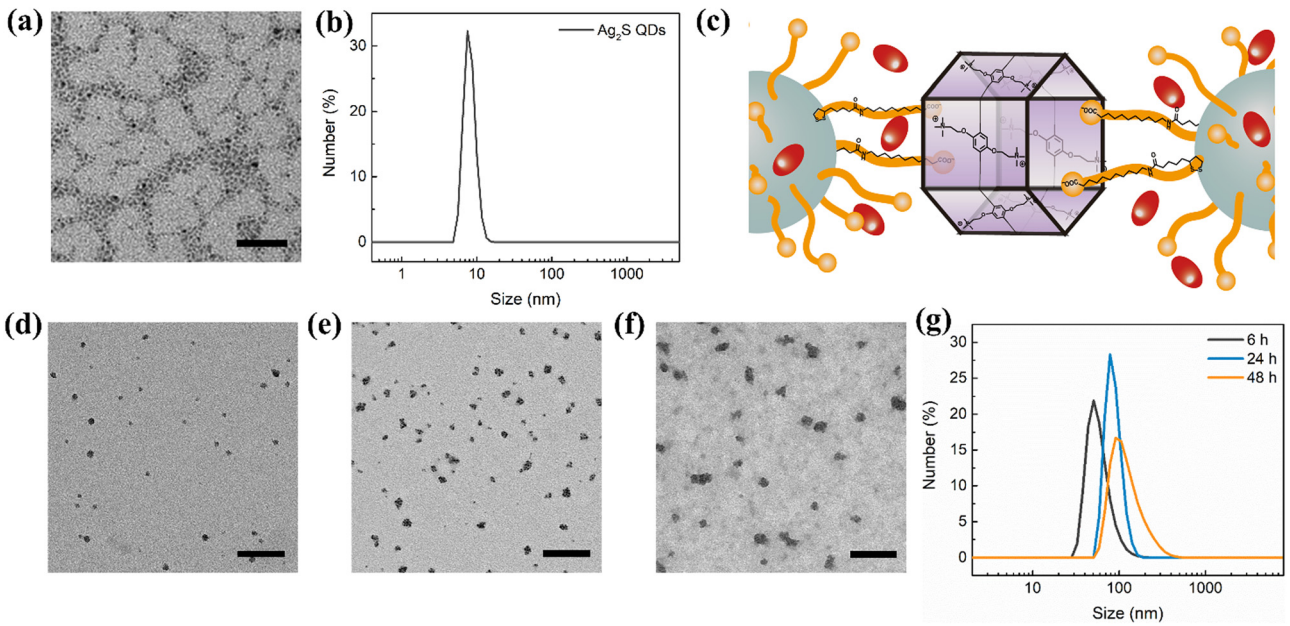

Fig. 1 Characterization of the Ag_2S-DOX-CP6 self-assembled co-delivery system. (a) TEM images of Ag_2S QDs with a scale bar of 25 nm. (b) Size distribution of Ag_2S QDs measured by DLS. (c) An illustration of the self-assembled nanostructures in Ag_2S-DOX-CP6 resulting from the interaction between CP6 and ligands on the surface of Ag_2S QDs. (d–f) TEM images of the co-delivery system at different drug-loading times: (d) 6 h, (e) 24 h, and (f) 48 h. Scale bar: 200 nm. (g) Size distribution of Ag_2S-DOX-CP6 nanoparticles with different drug-loading times measured by DLS at room temperature.

self-assembled approach and previous approaches is that the host–guest and hydrophobic interactions drive the self-assembly process based on small organic molecules.[10] To evaluate the drug-loading and -release capacity of this self-assembled nanocarrier as a controlled-release drug delivery system, we used DOX as the anticancer drug to co-self-assemble with the Ag_2S QDs and CP6 in PBS (pH 7.4). The encapsulation efficiency and loading efficiency of DOX were 50.7% and 10.2%, respectively. This self-assembled co-delivery system exhibited a high loading capacity for DOX, which was attributed to the hydrophobic interaction with DOX during self-assembly.

Unravelling the mechanism behind drug loading

To increase our understanding of the mechanism governing the drug loading directed by the co-assembled system, we investigated the morphological changes in the Ag_2S-DOX-CP6 system using TEM and DLS. The co-delivery system was monitored during the drug-loading process using TEM and DLS. Fig. 1d–f shows TEM images of the co-delivery system for different reaction times of self-assembly, and the size of the nanocarriers increased from approximately 10 nm to 80 nm with increasing reaction time. The size distribution of hydrodynamic diameters from DLS (Fig. 1g) was consistent with the TEM results. This suggests that the self-assembled nanostructures of Ag_2S-DOX-CP6 are highly size-dependent.

The TEM analysis showed that the resulting Ag_2S-DOX-CP6 nanocarriers were formed by the aggregation of several Ag_2S QDs, driven by the noncovalent interaction between the CP6 macrocycle and ligands on the surface of Ag_2S QDs. The noncovalent interaction responsible for the formation of Ag_2S-DOX-CP6 was elucidated using nuclear magnetic resonance (NMR). Because the NMR signal of ligands on the QDs was poor, a model compound of 11-AUA was used to analyze the noncovalent interaction between the macrocycle and Ag_2S QDs. The host–guest interaction between ligands on Ag_2S QDs and CP6 (CP6 $\supset$ 11-AUA) was studied by NMR spectra, and the signals of the methylene protons (H_{11}) exhibited remarkable downfield shifts, indicating the noncovalent interaction between CP6 and 11-AUA (Fig. S1, ESI†). The noncovalent interaction was also evidenced from the significant decrease of the UV-Vis absorbance peak at 289 nm of a phosphate buffer solution of CP6 (0.1 mM) when various concentrations of 11-AUA were introduced (Fig. S2, ESI†). Finally, two-dimensional nuclear Overhauser effect (2D NOESY) experiments were conducted to examine the spatial conformation of the resulting inclusion complex (Fig. S3, ESI†). Nuclear Overhauser effect (NOE) correlation signals were observed between protons H_a and H_b on the macrocycles and the methylene protons H_9, H_{10}, or H_{11} of 11-AUA, confirming the aforementioned interaction. These results revealed that the host–guest interaction induced the self-assembly of Ag_2S QDs.

DOX is typically buried in the hydrophobic pocket of liposomes, and we concluded that it was encapsulated by the alkyl chain of the ligands on the surface of the QDs during the noncovalent interaction between the macrocycle and the Ag_2S QDs.[29] The hydrodynamic diameter of the Ag_2S-CP6 nanoparticles was approximately 100 nm and increased to approximately 110 nm of the Ag_2S-DOX-CP6 nanoparticles from approximately 4 nm Ag_2S QDs through host–guest interaction after 48 h of reaction (in Fig. S4a–e, ESI†). As shown in Fig. S4d (ESI†), the high-resolution transmission electron microscopy (HRTEM) imaging of the Ag_2S-DOX-CP6 co-delivery system reveals that the resulting Ag_2S-DOX-CP6 nanocarriers were formed through the aggregation of several Ag_2S QDs. This aggregation was driven by the noncovalent interaction between the CP6 macrocycle and ligands on the surface of the Ag_2S QDs. The encapsulation of DOX indicates that DOX can affect the self-assembly process and was helpful for the formation of a well-dispersed delivery system. These findings suggest that this self-assembly strategy based on small molecule organics provides kinetic control over the complex co-self-assembly process, representing an approach to preparing nanocarriers that contain QDs and drugs for cancer treatment.[24]

Drug release and ROS generation by the co-delivery system

It was determined that the nanoparticles' hydrodynamic diameter was approximately 110 nm (Fig. S4e, ESI†), which meets the criteria for the enhanced permeability and retention (EPR) effect in tumor cells according to a previous report.[30] The stability of the co-delivery system in a physiological environment was tested using DLS (Fig. S4f, ESI†). The size distribution of Ag_2S-DOX-CP6 increased when dispersed in FBS compared to that in PBS and DMEM due to the formation of a protein corona on the surface of the nanostructures.[31] Nonetheless, the hydrodynamic diameter of Ag_2S-DOX-CP6 remained in the range of 200–250 nm, which would be considered suitable for delivery to tumor tissue *via* the EPR effect. The zeta potentials of Ag_2S QDs, Ag_2S-CP6, and Ag_2S-DOX-CP6 were −31.67 mV, −21.50 mV, and 5.16 mV, respectively (Fig. S4g, ESI†). The zeta potential of Ag_2S QDs increased after interaction with CP6, which was affected by quaternary ammonium groups, and became slightly positive after drug loading due to changes in the self-assembly process for Ag_2S QDs and CP6. This slightly positive electric charge is beneficial for nanoparticle uptake by cells.[32]

To further investigate their therapeutic applications, we characterized the nanoparticles' physicochemical properties (Fig. S5a and b, ESI†). The UV-Vis spectra of Ag_2S QDs, Ag_2S-CP6, DOX, and Ag_2S-DOX-CP6 were analyzed, and it showed an obvious absorption peak at 808 nm after self-assembly for Ag_2S-DOX-CP6. After loading DOX, the characteristic peak of DOX at 480 nm appeared, indicating successful drug loading in self-assembled nanostructures. Additionally, the fluorescence spectra of Ag_2S QDs, Ag_2S-CP6, DOX, and Ag_2S-DOX-CP6 were tested, showing that Ag_2S QDs emit no fluorescence under excitation by 480 nm light, which suggests that their photocatalytic performance may be excellent.

The release performance of Ag_2S-DOX-CP6 was evaluated in PBS solutions at pH values of 7.4 and 5.5 to assess its drug release characteristics. As shown in Fig. 2a, the accumulated release of DOX was 19.26% and 20.9% in PBS with a pH of 7.4 after 24 and 48 h, respectively, while at pH 5.5, the accumulative release was 43.1% and 52.1% after the same time intervals.

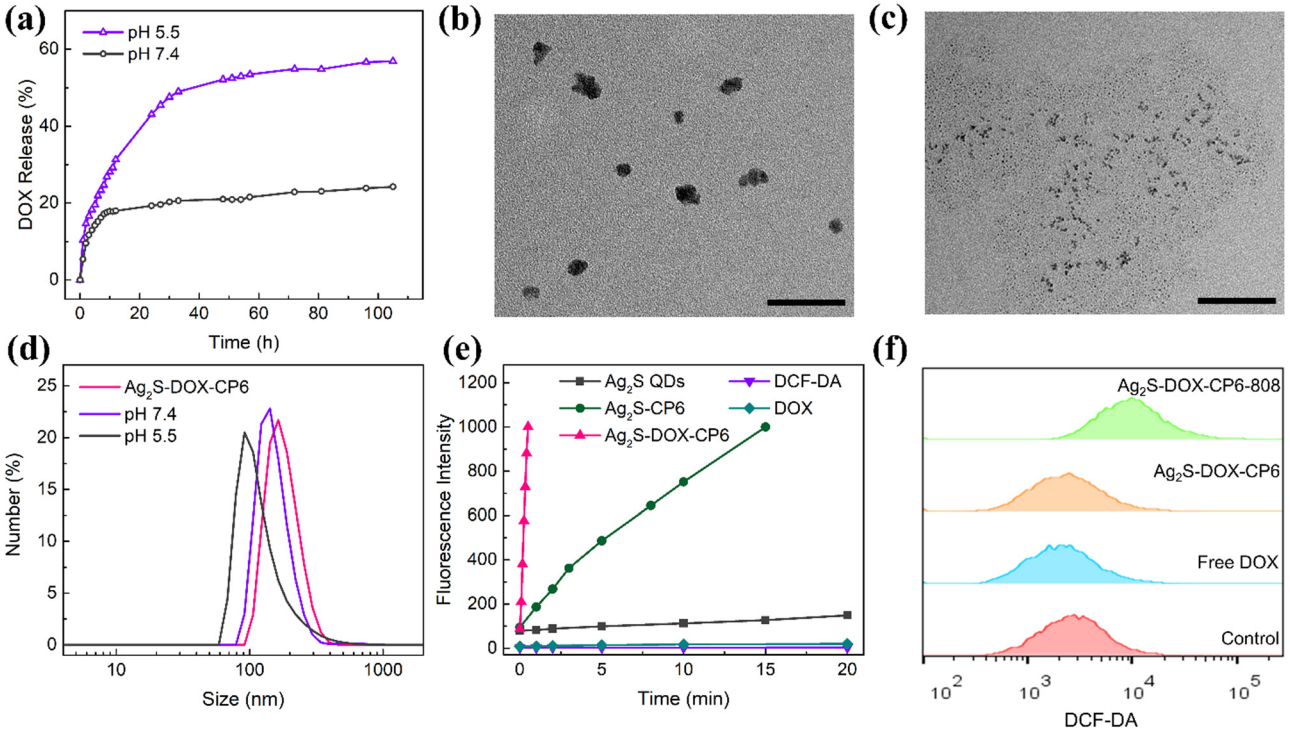

Fig. 2 Drug release and ROS generation performance of the co-delivery system. (a) DOX release curves of Ag_2S-DOX-CP6 nanoparticles in PBS (pH 7.4 and 5.5). (b and c) TEM images of Ag_2S-DOX-CP6 nanoparticles after drug release in PBS buffer of pH (b) 7.4 and (c) 5.5. Scale bar: 100 nm. (d) Size distributions of Ag_2S-DOX-CP6 samples after drug release in PBS buffer at 7.4 and 5.5, as measured by DLS. (e) ROS detection using a DCFH-DA probe under 808 nm irradiation (1.0 W cm^{-2}) for different samples. (f) Intracellular ROS detection of MCF-7 cells incubated with free DOX, Ag_2S-DOX-CP6, and Ag_2S-DOX-CP6 under 808 nm irradiation (1.0 W cm^{-2}, 1 min).

These results indicate that an acidic microenvironment can be used to control drug release from the co-delivery system, and pH-controlled drug release suggests its potential for cancer therapy, given the acidic environment of tumor cells.[33] The size distribution of the self-assembled nanocarriers after drug release was also investigated using TEM and DLS, as shown in Fig. 2b–d. It was observed that the nanoparticle size sharply decreased after drug release at pH 5.5, suggesting that the co-delivery system disassembled into smaller sizes. This feature can enable intelligent control of chemotherapy to achieve more efficient drug delivery to tumor sites.[21]

Moreover, the ability of Ag_2S-DOX-CP6 to generate ROS under 808 nm NIR laser irradiation was evaluated using 2,7-dichlorodihydrofluorescein diacetate (DCFH-DA) as a fluorescence probe. As shown in Fig. 2e, the amount of ROS generated increased with the irradiation time, indicating that all Ag_2S nanoparticles participated in photocatalytic activities under NIR excitation.[34] Furthermore, the ability of self-assembled hybrid nanoparticles to generate ROS, especially Ag_2S-DOX-CP6 after drug loading, was significantly enhanced due to the presence of CP6 and DOX. Simultaneously, various ROS were separately detected using different probes, as shown in Fig. S6 (ESI†). It was determined that singlet oxygen ($^1O_2$) was the primary ROS produced during the NIR irradiation process. This can be attributed to the fact that CP6 and DOX altered electronic transmission and separation during irradiation, leading to the trapping of unpaired electrons and increased ROS generation during the photocatalytic process.[35]

The enhanced photocatalytic activity of the Ag_2S-DOX-CP6 nanoparticles suggested their potential as excellent photosensitizers in PDT. To further confirm this, intracellular ROS generation in MCF-7 breast cancer cells incubated with Ag_2S-DOX-CP6 (50 μg mL^{-1}) was investigated using flow cytometry and confocal laser scanning microscopy (CLSM), as shown in Fig. 2f and Fig. S7 (ESI†). The fluorescence of DCF increased in MCF-7 cells with the irradiation of an 808 nm NIR laser, indicating an increase in ROS generation. These results suggest that the co-delivery system could be used as an effective photosensitizer in PDT, enabling highly effective PDT under NIR light irradiation.

In vitro cytotoxicity and cellular uptake of co-delivery systems

The biocompatibility of nanoplatforms is an essential consideration for any drug delivery system.[25] To assess the cytotoxicity of the co-delivery nanocarriers, we performed the thiazolyl blue tetrazolium bromide (MTT) assay.[33] Fig. 3a shows the viabilities of MCF-7 cells after 24 h incubation with Ag_2S QDs and Ag_2S-CP6 nanoparticles at concentrations ranging from 0.5 to 30 μg mL^{-1}. The viabilities of MCF-7 cells remained above 80% for Ag_2S-CP6 nanoparticles, indicating low cytotoxicity. Based on the MTT results, the co-delivery system exhibited excellent biocompatibility for delivering drugs to tumor cells.

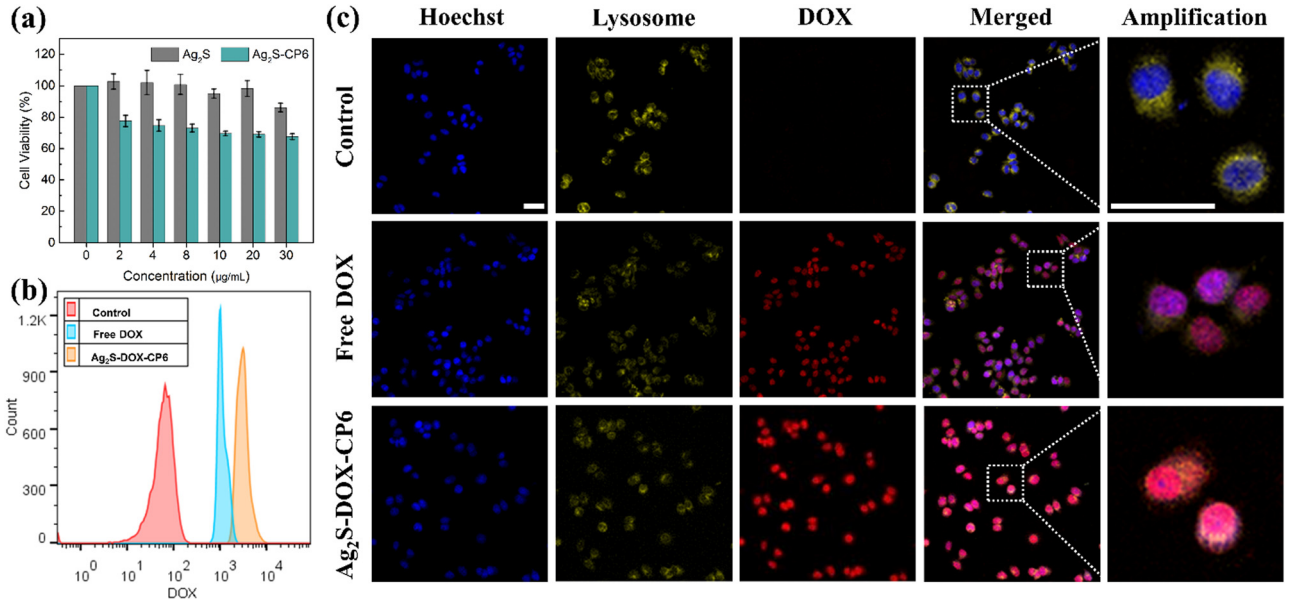

Fig. 3 (a) *In vitro* biocompatibility of Ag_2S QDs and Ag_2S-CP6 at different concentrations incubated with MCF-7 cells. (b) Flow cytometry curves of MCF-7 cells incubated with free DOX and Ag_2S-DOX-CP6 nanoparticles by measuring DOX fluorescence using the PerCP channel. (c) CLSM images of MCF-7 cells incubated with free DOX and Ag_2S-DOX-CP6 (DOX concentration: 5 μg mL^{-1}) for 60 min. The MCF-7 cells incubated without any drugs were used as a control. The cells were treated with Hoechst 33342 and LysoTracker Deep Red to stain the nucleus and lysosome. DOX was excited at the wavelength of 488 nm, and the fluorescence images were captured at emission wavelengths of 550–640 nm. Scale bar: 50 μm.

DOX is known to inhibit nucleic acid synthesis, and thus it is an effective antitumor agent.[29] Even after release into the cell nucleus, DOX continues to exert antitumor activity.[36,37] In the current study, flow cytometry and CLSM were utilized to observe the cellular uptake capability of Ag_2S-DOX-CP6 nanoparticles and their localization in MCF-7 cells. The uptake of Ag_2S-DOX-CP6 nanoparticles in MCF-7 cells was evaluated using flow cytometry, as shown in Fig. 3b. The DOX fluorescence intensity in the Ag_2S-DOX-CP6 group was found to be stronger than that of the free DOX group, indicating that the nanoparticles were more easily taken up and accumulated in the co-delivery system as compared to free DOX in MCF-7 cells. Additionally, CLSM was used to observe the process of cellular uptake of and drug release by Ag_2S-DOX-CP6 nanoparticles in MCF-7 cells (DOX can easily enter the nuclei of MCF-7 cells) in Fig. S8 and S9 (ESI†). Additionally, the cellular uptake of Ag_2S-DOX-CP6 increased with increasing incubation time for the samples exposed to Ag_2S-DOX-CP6 nanoparticles. Consistent with the flow cytometry results, there was greater accumulation of Ag_2S-DOX-CP6 nanoparticles in MCF-7 cells as compared to free DOX, as shown in Fig. 3c. These results demonstrated the superb potential of the self-assembled Ag_2S-DOX-CP6 nanoparticles to become a co-delivery system candidate.

In vitro chemo-photodynamic therapy

The Ag_2S-DOX-CP6 nanoparticles were evaluated for their chemo-photodynamic synergistic therapy performance *in vitro* using the MTT assay.[38] The CHT performance was evaluated first, and the viabilities of MCF-7 cells incubated with free DOX and Ag_2S-DOX-CP6 nanoparticles were tested for 24, 48, and 72 h. As shown in Fig. 4a and b, the viabilities of MCF-7 cells incubated with Ag_2S-DOX-CP6 nanoparticles were lower than those incubated with free DOX at a similar DOX concentration. The half maximal inhibitory concentration (IC_{50}) values for free DOX and Ag_2S-DOX-CP6 nanoparticles were 2.728 μg mL^{-1} and 0.786 μg mL^{-1} in MCF-7 cells (Fig. 4d), respectively, indicating that there was a greater chemotherapy effect against cancer by the co-delivery system of Ag_2S-DOX-CP6.

Furthermore, the combined chemo-photodynamic therapy performances of Ag_2S-DOX-CP6 were studied, and the results are shown in Fig. 4c. Under NIR laser irradiation, the viability of MCF-7 cells for the Ag_2S-DOX-CP6 group decreased to 8.8%, compared to 39.0% for cells incubated with Ag_2S-CP6 and without DOX under the same laser conditions. The viability was 24.2% for MCF-7 cells exposed to Ag_2S-DOX-CP6 nanoparticles without irradiation. In addition, the IC_{50} of Ag_2S-DOX-CP6 nanoparticles under NIR light was approximately 11.9 times lower than that of free DOX in MCF-7 cells (Fig. 4d). These findings indicated that there was significant anti-tumor efficacy in chemo-photodynamic treatment for breast cancer.

Dead/live cell imaging was performed for cells treated with Ag_2S-DOX-CP6 under 808 nm irradiation to evaluate their anti-tumor ability, as shown in Fig. 4e. In this experiment, MCF-7 cells were incubated with different samples (DOX concentration: 5 μg mL^{-1}) for 8 h with or without 808 nm irradiation (1.0 W cm^{-2}, 1 min). Low DOX concentration reduced the interference of DOX fluorescence on PI fluorescence in dead/live cell imaging tests. The amount of living cells can also be used to evaluate the anti-tumor ability of Ag_2S-DOX-CP6 with NIR light. The number of living cells in the Ag_2S-DOX-CP6-808 group was far less than that in other groups, which is consistent with the results from the MTT assay, and further proves the

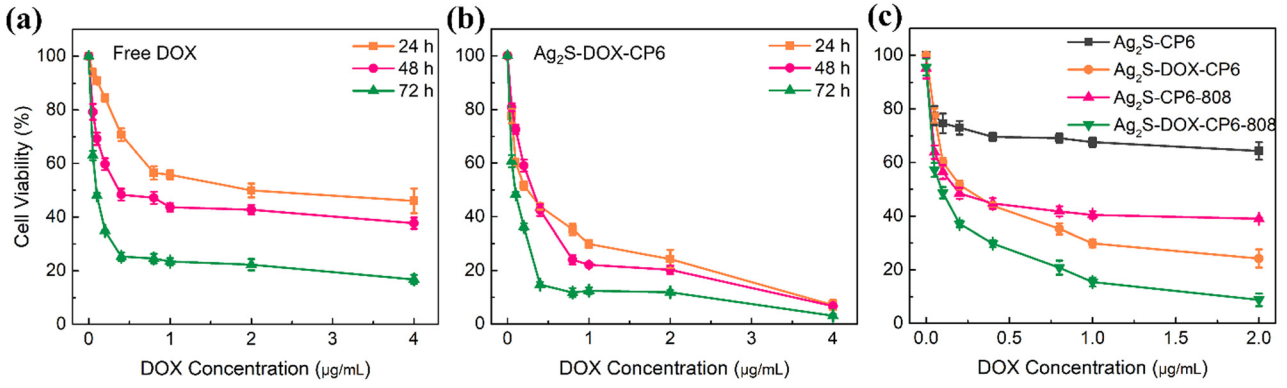

(d)

Samples	Free DOX	Ag_2S-DOX-CP6	Ag_2S-DOX-CP6-808
IC_{50} (μg/mL)	2.728	0.786	0.229

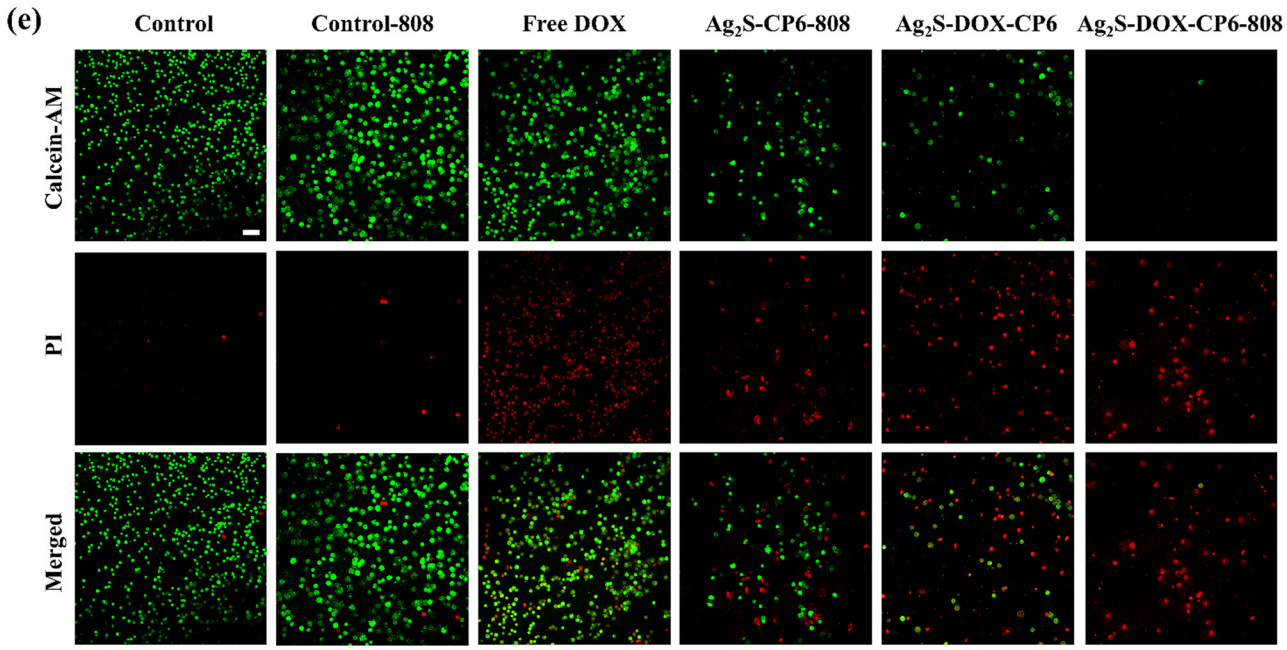

Fig. 4 (a–c) Cell viabilities of MCF-7 cells incubated with free DOX, Ag_2S-DOX-CP6, and Ag_2S-DOX-CP6 under 808 nm irradiation (1.0 W cm^{-2}, 20 s). (d) The calculated IC_{50} of free DOX and Ag_2S-DOX-CP6 nanoparticles in MCF-7 cells. (e) Fluorescence images of MCF-7 cells incubated with different samples (DOX concentration: 5 μg mL^{-1}) with or without 808 nm irradiation (1.0 W cm^{-2}, 1 min). The MCF-7 cells were treated with calcein-AM and PI dyes to stain live and dead cells. PI was excited at the wavelength of 488 nm, and emission wavelengths were at 630–680 nm. Scale bar: 100 μm.

excellent chemo-photodynamic therapeutic ability of Ag_2S-DOX-CP6 in MCF-7 cells. In addition, cell apoptosis in MCF-7 cells induced by Ag_2S-DOX-CP6 nanoparticles was investigated by flow cytometry, as shown in Fig. S10 (ESI†). The early and later apoptotic cells constituted 9.08 ± 0.99% and 5.46 ± 0.67% when the MCF-7 cells were treated with free DOX and Ag_2S-DOX-CP6, whereas they increased to 14.87 ± 2.03% when the cells were incubated with Ag_2S-DOX-CP6 and treated with NIR light. Thus, there was a slightly lower amount of apoptotic cells from the Ag_2S-DOX-CP6 group as compared to the group that was treated with free DOX, because most cells were already dead due to the cytotoxicity of Ag_2S-DOX-CP6.

Thus, Ag_2S-DOX-CP6 nanoparticles, when combined with NIR irradiation, exhibited superior anticancer activity compared to free DOX alone, resulting in apoptosis-induced inhibition of tumor cell proliferation. This demonstrates the successful design and development of a combined photocatalytic and drug delivery system for chemo-photodynamic synergistic therapy in MCF-7 cells. The promising potential of this approach highlights the possibility of a more effective method for inhibiting tumor proliferation.

In vivo biocompatibility and chemo-photodynamic therapy

To assess the potential of the self-assembled co-delivery system in cancer therapy, the *in vivo* biocompatibility of Ag_2S-DOX-CP6

was evaluated in Institute of Cancer Research (ICR) mice. Following the tail vein injection of free DOX and Ag_2S-DOX-CP6, the major organs of mice were subjected to hematoxylin-eosin (H&E) staining to examine organ pathology (Fig. S11, ESI†). In the group treated with free DOX, minor leukocyte infiltration was observed in the alveolar regions of the heart and lung. By contrast, no significant pathological lesions were found in the heart, liver, spleen, lung, or kidney of mice treated with Ag_2S-DOX-CP6, indicating that this co-delivery system can mitigate the toxicity of DOX.[39] Therefore, this stimuli-responsive co-delivery system showed excellent biocompatibility, suggesting its potential for cancer treatment.

To monitor the accumulation of the co-delivery system, a NIR fluorescent dye IR-783 was loaded into the system. *In vivo* biodistribution and *in vitro* fluorescence images of tumors and major organs from MCF-7 tumor-bearing mice following injection of free IR-783 and Ag_2S-DOX-CP6 labeled with IR-783 (Ag_2S-DOX-CP6-783) are presented in Fig. S12 (ESI†). The fluorescence intensity of the tumor in the Ag_2S-DOX-CP6-783 group increased over time, peaking at 24 h and remaining high for several days, as shown in Fig. S12a and b (ESI†). This indicated that Ag_2S-DOX-CP6 exhibited exceptional tumor accumulation ability. As displayed in Fig. S12c and d (ESI†), *in vitro* fluorescence images of tumors and major organs at 24 h post-injection revealed that the tumor accumulation of Ag_2S-DOX-CP6 nanoparticles was significantly higher compared to the free IR-783 group, further confirming their ability to accumulate in tumors. These findings demonstrate that the co-delivery system

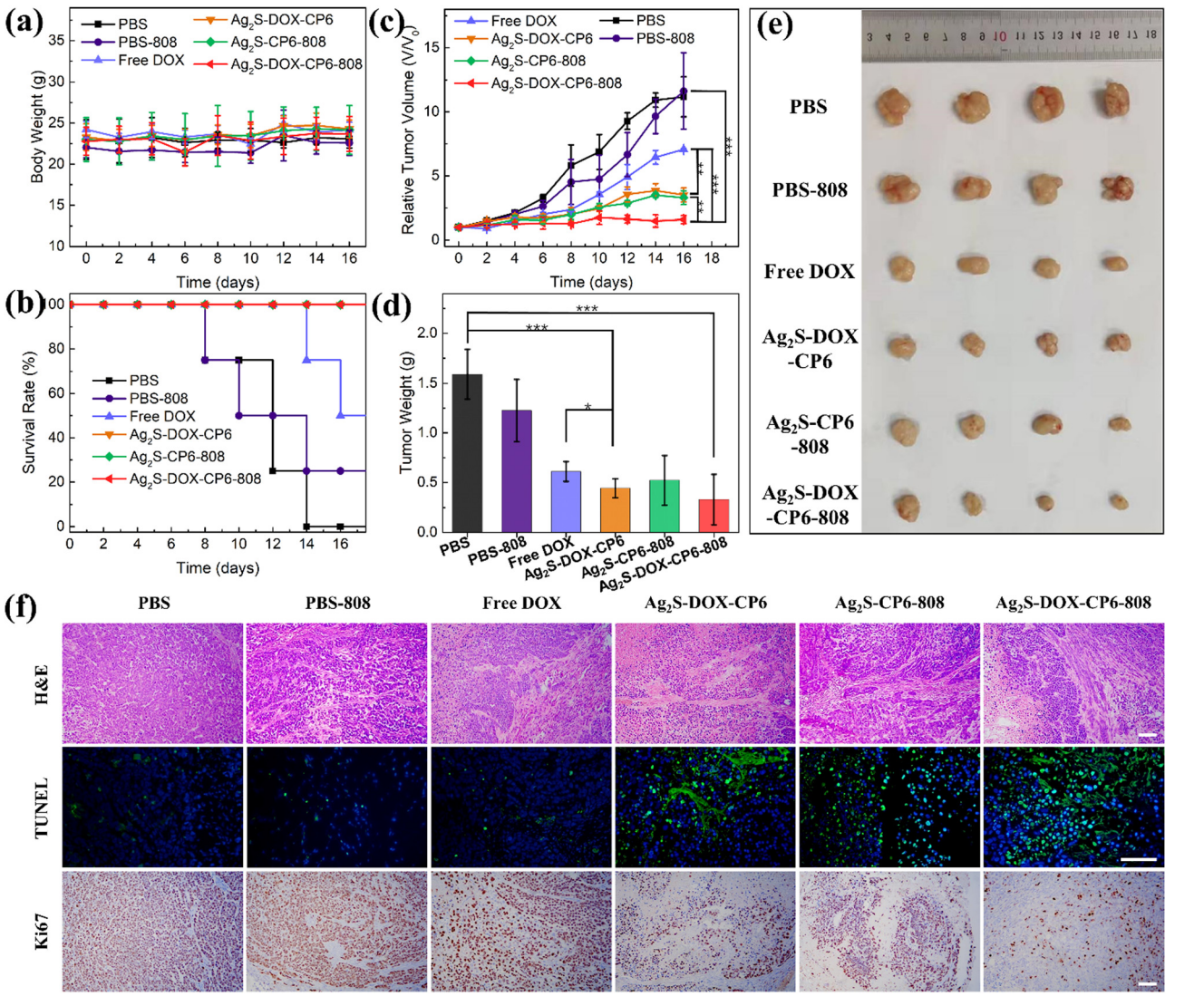

Fig. 5 Anti-tumor efficacies of Ag_2S-CP6 and Ag_2S-DOX-CP6 with or without irradiation (2.0 W cm^{-2}, 5 min) in BALB/c-nu tumor mice (n = 4, *p < 0.05, **p < 0.01, ***p < 0.001). PBS with or without 808 nm irradiation, and free DOX were used as control groups. (a) Changes in the body weight of MCF-7 tumor-bearing mice during the treatments with PBS, PBS-808, free DOX, Ag_2S-DOX-CP6, Ag_2S-CP6-808, and Ag_2S-DOX-CP6-808. (b) Survival curve of tumor-bearing mice after different treatments with various formulations. (c) Relative tumor growth curves during treatment with various formulations. (d and e) Tumor weight and tumor photograph after different treatments. (f) H&E, TUNEL, and Ki-67 staining of tumors in various formulations after 12 days of treatments. Scale bar: 100 μm.

possessed excellent biocompatibility and strong tumor accumulation capability, and therefore it is a promising candidate for cancer treatment.

To further validate the excellent antitumor efficacy observed *in vitro*, the anti-tumor effect of the self-assembled co-delivery system was evaluated using a xenograft model of MCF-7 cells in BALB/c-nu mice (n = 4). The mice were treated with free DOX, Ag_2S-DOX-CP6, or PBS three times on days 0, 4, and 8, and were then subjected to irradiation with an 808 nm laser on the day following tail vein injection. The mice were monitored every 2 days for changes in body weight and tumor volume, as shown in Fig. 5a–c. There was no significant evidence of weight loss or death of mice in the Ag_2S-DOX-CP6 or Ag_2S-DOX-CP6-808 groups during the treatment (Fig. 5b), indicating the excellent biocompatibility and safety of the nanoplatform during the treatment period.[40] Moreover, it was observed that the relative tumor volumes in the mice treated with PBS sharply and uncontrollably increased, as shown in Fig. 5c. In contrast, those tumor-bearing mice treated with Ag_2S-DOX-CP6 exhibited slower tumor growth as compared to the free DOX group, indicating the remarkable chemotherapeutic effect of this self-assembled co-delivery system. Under irradiation with the 808 nm laser, there was significantly enhanced anti-cancer efficacy for the group treated with Ag_2S-DOX-CP6-808 as compared to the free DOX group and Ag_2S-DOX-CP6 group. These results were further supported by tumor weights and images, as shown in Fig. 5d and e. Notably, the mice receiving Ag_2S-DOX-CP6-808 treatment exhibited the strongest tumor inhibition capacity, confirming the synergism of chemo-photodynamic therapy.

Furthermore, to investigate the anti-tumor effects of Ag_2S-DOX-CP6, we performed H&E staining, terminal deoxynucleotidyl transferase dUTP nick-end labeling (TUNEL) staining, and Ki-67 protein staining of tumor slices, as shown in Fig. 5f. The results showed that treatment with Ag_2S-DOX-CP6 and 808 nm laser induced additional apoptosis and necrosis compared to other treatments, indicating the effectiveness of CHT and PDT in inhibiting tumor growth.[41] These findings confirmed that the co-delivery system under NIR irradiation exhibited the strongest tumor inhibition ability, demonstrating the synergistic therapy of CHT and PDT for cancer.

To evaluate the potential systemic toxicity of Ag_2S-DOX-CP6 in BALB/c-nu mice, we analyzed standard hematology markers, as shown in Fig. S13 (ESI†).[42] The results revealed no significant differences in routine blood test indexes between the group treated with Ag_2S-DOX-CP6 and 808 nm laser and the other treatment groups. Together, these results confirmed the excellent biocompatibility of the co-delivery system, and reinforced its potential as a drug delivery system for the chemo-photodynamic treatment of cancer.

Conclusions

In summary, we developed a self-assembled co-delivery system (Ag_2S-DOX-CP6) to increase the efficiency of PDT and stimuli-responsive payload release for chemo-photodynamic therapy of cancer. By utilizing host-guest interactions, we were able to engineer the self-assembly of the PSs of Ag_2S QDs and CP6 into ordered nanostructures. During this process, we took advantage of the high surface area-to-volume ratio of Ag_2S QDs to produce ample hydrophobic spaces to accommodate DOX molecules with a drug-loading efficiency of 10.2%. In a PBS solution at pH 5.5, the amount of DOX released reached 43.1% and 52.1% after 24 h and 48 h, respectively, indicating the system's ability to intelligently release drugs in the acidic microenvironment of tumor cells. Furthermore, Ag_2S QDs exhibited high catalytic activity under NIR light and demonstrated outstanding PDT ability based on the results of extracellular and intracellular ROS generation.

Ag_2S QDs were used as PSs to generate ROS under 808 nm NIR light, and they were also applied as nanocarriers to increase the efficiency of delivering hydrophobic anticancer drugs to the tumor. The uptake assessment of CLSM images and flow cytometry indicated that there was greater accumulation of Ag_2S-DOX-CP6 nanoparticles in MCF-7 cells, where they were delivered and released DOX into the nucleus to achieve effective CHT. Moreover, when combined with NIR light, the Ag_2S-DOX-CP6 treatment reduced the viability of MCF-7 cells to 8.8% (compared to the free DOX group of 49.91% with DOX concentration of 2 μg mL^{-1}).

The anti-tumor effect and biocompatibility of Ag_2S-DOX-CP6 were confirmed *in vivo*. In addition, H&E staining and hematology analysis of the major organs of mice revealed low side effects and satisfactory biocompatibility of the co-delivery system. These results suggest that there is great potential for the co-delivery system as a drug delivery system for chemo-photodynamic cancer treatment, and it could serve as a nanoplatform that co-delivers PSs and drugs to tumor sites while offering a synergistic effect of chemo-photodynamic therapy.

Author contributions

Concept, design, and research direction: J. L. and A. W. Material and nanostructure preparation: X. W. Experiments and characterization: X. W., J. Y., J. X., Y. L., R. Z., X. W., J. Y., D. Z., D. Q., and G. S. Manuscript writing: X. W. and J. L.

Conflicts of interest

The authors declare no competing financial interests.

Acknowledgements

This work is financially supported by the National Natural Science Foundation of China (No. 22161016, 82202274, 82072032, 32025021, 52002380, 31971292), Ningbo 3315 Innovative Teams Program (Grant No. 2019A-14-C), the Sigrid Jusélius Foundation (senior researcher fellowship) and the Academy of Finland (318524, 355798), Fellowship of China Postdoctoral Science Foundation (2021M692872, 2022M723206),

the member of Youth Innovation Promotion Association Foundation of CAS, China (2023310), and the Provincial Natural Science Foundation of Zhejiang (LQ23H180003). Markus Peurla (Laboratory Engineer, Institute of Biomedicine) and Cell Imaging and Cytometry Core (Turku Bioscience Centre, Turku, Finland) are acknowledged for their assistance with the TEM characterization and imaging/flow cytometry analysis.

References

1 R. Zheng, S. Zhang, H. Zeng, S. Wang, K. Sun, R. Chen, L. Li, W. Wei and J. He, *J. Natl. Cancer Cent.*, 2022, **2**, 1–9.
2 X. Li, J. F. Lovell, J. Yoon and X. Chen, *Nat. Rev. Clin. Oncol.*, 2020, **17**, 657–674.
3 S. Zhang, J. Wang, Z. Kong, X. Sun, Z. He, B. Sun, C. Luo and J. Sun, *Biomaterials*, 2022, **282**, 121433.
4 N. Kwon, H. Kim, X. Li and J. Yoon, *Chem. Sci.*, 2021, **12**, 7248–7268.
5 R. Keerthiga, Z. Zhao, D. Pei and A. Fu, *ACS Biomater. Sci. Eng.*, 2020, **6**, 5474–5485.
6 Z. Wang, N. Little, J. Chen, K. T. Lambesis, K. T. Le, W. Han, A. J. Scott and J. Lu, *Nat. Nanotechnol.*, 2021, **16**, 1130–1140.
7 H. Sung, J. Ferlay, R. L. Siegel, M. Laversanne, I. Soerjomataram, A. Jemal and F. Bray, *Ca-Cancer J. Clin.*, 2021, **71**, 209–249.
8 X.-Y. Hu, J. Gao, F.-Y. Chen and D.-S. Guo, *J. Controlled Release*, 2020, **324**, 124–133.
9 X. Zhao, J. Liu, J. Fan, H. Chao and X. Peng, *Chem. Soc. Rev.*, 2021, **50**, 4185–4219.
10 Q. Qi, X. Zeng, L. Peng, H. Zhang, M. Zhou, J. Fu and J. Yuan, *J. Biomater. Sci., Polym. Ed.*, 2020, **31**, 1385–1404.
11 U. Badilli, F. Mollarasouli, N. K. Bakirhan, Y. Ozkan and S. A. Ozkan, *TrAC, Trends Anal. Chem.*, 2020, **131**, 116013.
12 Y. W. Jiang and B. Z. Tian, *Nat. Rev. Mater.*, 2018, **3**, 473–490.
13 H. Zhang, T. Wang, H. Liu, F. Ren, W. Qiu, Q. Sun, F. Yan, H. Zheng, Z. Li and M. Gao, *Nanoscale*, 2019, **11**, 7600–7608.
14 J. Wankar, N. G. Kotla, S. Gera, S. Rasala, A. Pandit and Y. A. Rochev, *Adv. Funct. Mater.*, 2020, **30**, 1909049.
15 K. Cheng, X.-Q. Yang, X.-S. Zhang, J. Chen, J. An, Y.-Y. Song, C. Li, Y. Xuan, R.-Y. Zhang, C.-H. Yang, X.-L. Song, Y.-D. Zhao and B. Liu, *Adv. Mater.*, 2018, **28**, 1803118.
16 D. Ling, W. Park, S.-J. Park, Y. Lu, K. S. Kim, M. J. Hackett, B. H. Kim, H. Yim, Y. S. Jeon, K. Na and T. Hyeon, *J. Am. Chem. Soc.*, 2014, **136**, 5647–5655.
17 D. Wu, B. L. Li, Q. Zhao, Q. Liu, D. Wang, B. He, Z. Wei, D. T. Leong, G. Wang and H. Qian, *Small*, 2020, **16**, 1906975.
18 J. V. Rival, N. Nonappa and E. S. Shibu, *ACS Appl. Mater. Interfaces*, 2020, **12**, 14569–14577.
19 C. Wang, H. Li, J. Dong, Y. Chen, X. Luan, X. Li and X. Du, *Chem. – Eur. J.*, 2022, **28**, e202202050.
20 Q. Yang, W. Xu, M. Cheng, S. Zhang, E. G. Kovaleva, F. Liang, D. Tian, J.-A. Liu, R. M. Abdelhameed, J. Cheng and H. Li, *Chem. Commun.*, 2022, **58**, 3255–3269.
21 C. B. Yang, Z. I. Lin, J. A. Chen, Z. R. Xu, J. Y. Gu, W. C. Law, J. H. C. Yang and C. K. Chen, *Macromol. Biosci.*, 2021, **22**, 2100349.
22 A. S. Braegelman and M. J. Webber, *Theranostics*, 2019, **9**, 3017–3040.
23 X. Liu, K. Jia, Y. Wang, W. Shao, C. Yao, L. Peng, D. Zhang, X.-Y. Hu and L. Wang, *ACS Appl. Mater. Interfaces*, 2017, **9**, 4843–4850.
24 G. Yu, J. Zhou, J. Shen, G. Tang and F. Huang, *Chem. Sci.*, 2016, **7**, 4073–4078.
25 S. Chao, Z. Shen, Y. Pei, Y. Lv, X. Chen, J. Ren, K. Yang and Z. Pei, *Chem. Commun.*, 2021, **57**, 7625–7628.
26 W. Jiang, Z. Wu, X. Yue, S. Yuan, H. Lu and B. Liang, *RSC Adv.*, 2015, **5**, 24064–24071.
27 H. Jia, W. He, W. G. Wamer, X. Han, B. Zhang, S. Zhang, Z. Zheng, Y. Xiang and J.-J. Yin, *J. Phys. Chem. C*, 2014, **118**, 21447–21456.
28 X. Wu, J. Liu, L. Yang and F. Wang, *Colloids Surf., B*, 2019, **175**, 239–247.
29 S. Li, Y. Gao, Y. Ding, A. Xu and H. Tan, *Chin. Chem. Lett.*, 2021, **32**, 313–318.
30 Y. Zhang, M. Y. Li, X. M. Gao, Y. H. Chen and T. Liu, *J. Hematol. Oncol.*, 2019, **12**, 137.
31 K. Aslan, I. Gryczynski, J. Malicka, E. Matveeva, J. R. Lakowicz and C. D. Geddes, *Curr. Opin. Biotech.*, 2005, **16**, 55–62.
32 X. Wu, L. Luo, S. Yang, X. Ma, Y. Li, C. Dong, Y. Tian, L. E. Zhang, Z. Shen and A. Wu, *ACS Appl. Mater. Interfaces*, 2015, **7**, 9965–9971.
33 Y. Pan, L. e Zhang, L. Zeng, W. Ren, X. Xiao, J. Zhang, L. Zhang, A. Li, G. Lu and A. Wu, *Nanoscale*, 2016, **8**, 878–888.
34 D.-W. Zheng, B. Li, C.-X. Li, J.-X. Fan, Q. Lei, C. Li, Z. Xu and X.-Z. Zhang, *ACS Nano*, 2016, **10**, 8715–8722.
35 X. Wu, L. Yang, L. Luo, G. Shi, X. Wei and F. Wang, *ACS Appl. Bio Mater.*, 2019, **2**, 1998–2005.
36 R. K. Kankala, C. G. Liu, A. Z. Chen, S. B. Wang, P. Y. Xu, L. K. Mende, C. L. Liu, C. H. Lee and Y. F. Hu, *ACS Biomater. Sci. Eng.*, 2017, **3**, 2431–2442.
37 G. Lin, P. Mi, C. C. Chu, J. Zhang and G. Liu, *Adv. Sci.*, 2016, **3**, 1600134.
38 J. Han, H. Xia, Y. Wu, S. N. Kong, A. Deivasigamani, R. Xu, K. M. Hui and Y. Kang, *Nanoscale*, 2016, **8**, 7861–7865.
39 Y. Cao, J. Yang, D. Eichin, F. Zhao, D. Qi, L. Kahari, C. Jia, M. Peurla, J. M. Rosenholm, Z. Zhao, S. Jalkanen and J. Li, *Angew. Chem., Int. Ed.*, 2021, **60**, 3062–3070.
40 Z. Shen, T. Chen, X. Ma, W. Ren, Z. Zhou, G. Zhu, A. Zhang, Y. Liu, J. Song, Z. Li, H. Ruan, W. Fan, L. Lin, J. Munasinghe, X. Chen and A. Wu, *ACS Nano*, 2017, **11**, 10992–11004.
41 H. Li, K. Qian, H. Zhang, L. Li, L. Yan, S. Geng, H. Zhao, H. Zhang, B. Xiong, Z. Li, C. Zheng, Y. Zhao and X. Yang, *Chem. Eng. J.*, 2021, **418**, 129534.
42 X.-D. Zhang, D. Wu, X. Shen, P.-X. Liu, F.-Y. Fan and S.-J. Fan, *Biomaterials*, 2012, **33**, 4628–4638.

